



Mammogram synthesis using a 3D simulation. I. Breast tissue model and image acquisition simulation

Predrag R. Bakic, Michael Albert, Dragana Brzakovic, and Andrew D. A. Maidment

Citation: *Medical Physics* **29**, 2131 (2002); doi: 10.1118/1.1501143

View online: <http://dx.doi.org/10.1118/1.1501143>

View Table of Contents: <http://scitation.aip.org/content/aapm/journal/medphys/29/9?ver=pdfcov>

Published by the American Association of Physicists in Medicine

Articles you may be interested in

Detection of masses in digital breast tomosynthesis using complementary information of simulated projection
Med. Phys. **42**, 7043 (2015); 10.1118/1.4935533

Computerized nipple identification for multiple image analysis in computer-aided diagnosis
Med. Phys. **31**, 2871 (2004); 10.1118/1.1800713

Mammogram synthesis using a three-dimensional simulation. III. Modeling and evaluation of the breast ductal network

Med. Phys. **30**, 1914 (2003); 10.1118/1.1586453

Mammogram synthesis using a 3D simulation. II. Evaluation of synthetic mammogram texture

Med. Phys. **29**, 2140 (2002); 10.1118/1.1501144

Automated registration of breast lesions in temporal pairs of mammograms for interval change analysis—local affine transformation for improved localization

Med. Phys. **28**, 1070 (2001); 10.1118/1.1376134

Educational Lectures

Don't miss these fascinating in-booth speakers. Lectures will be held throughout the show during exhibit hours only, in booth #4001.

Joe Ting, PhD

Utilizing EPID for stereotactic cone commissioning and verification in RIT

Sam Hancock, PhD

Isocenter optimization tools for LINAC-based SRS/SBRT

AAPM 2016 Learn and Earn



Users Meeting

Enjoy some delicious dessert while you learn and earn 2 CAMPEP credit hours at our Users Meeting.

Location . . . Marriott Marquis, Washington, DC

Date . . . Sunday, July 31

Time . . . 7-9 PM

Visit us at AAPM Booth #4001



call or visit
719.590.1077 • radimage.com

© 2015 Radimage Imaging Technologies, Inc.
2015-01-06

Mammogram synthesis using a 3D simulation.

I. Breast tissue model and image acquisition simulation

Predrag R. Bakic and Michael Albert

Department of Radiology, Thomas Jefferson University, Suite 3390, Gibbon Building, 111 South 11th Street, Philadelphia, Pennsylvania 19107-5563

Dragana Brzakovic

Office of Integrative Activities, National Science Foundation, Arlington, Virginia 22230

Andrew D. A. Maidment^{a)}

Department of Radiology, Thomas Jefferson University, Suite 3390, Gibbon Building, 111 South 11th Street, Philadelphia, Pennsylvania 19107-5563

(Received 25 February 2002; accepted for publication 14 June 2002; published 27 August 2002)

A method is proposed for generating synthetic mammograms based upon simulations of breast tissue and the mammographic imaging process. A computer breast model has been designed with a realistic distribution of large and medium scale tissue structures. Parameters controlling the size and placement of simulated structures (adipose compartments and ducts) provide a method for consistently modeling images of the same simulated breast with modified position or acquisition parameters. The mammographic imaging process is simulated using a compression model and a model of the x-ray image acquisition process. The compression model estimates breast deformation using tissue elasticity parameters found in the literature and clinical force values. The synthetic mammograms were generated by a mammogram acquisition model using a monoenergetic parallel beam approximation applied to the synthetically compressed breast phantom. © 2002 American Association of Physicists in Medicine. [DOI: 10.1118/1.1501143]

Key words: mammography simulation, 3D, breast tissue, mammographic compression, x-ray image acquisition

I. INTRODUCTION

Visibility of breast lesions in mammography is compromised by overlapping projections of normal anatomic structures that generate a background texture, which can mask existing abnormalities or introduce false ones. Several authors^{1–3} have shown that these parenchymal patterns are often the limiting factor in detection tasks. A 3D simulation of mammography is proposed to provide insight into the formation of such patterns. The simulation allows one to analyze the correlation between the 3D composition of the breast and its 2D mammographic appearance. By identifying the dominant anatomical structures found in an average breast, this model can help analyze the deformation of those structures during the exam and their appearance in mammograms. A 3D mammography simulation can also serve as a complement to experiments with respect to positioning, compression, and acquisition. Optimization of imaging parameters (such as compression angle and force, x-ray tube kVp and mAs, etc.) cannot be achieved by repeatedly imaging the same patient, due to concerns about the radiation dose. Such simulations can also be useful in training medical personnel by demonstrating the effects of technique selection on image quality or by determining 3D lesion position from two or more projections. Finally, a 3D breast model can provide a theoretical framework for testing new breast imaging modalities. Many new modalities are being developed today, including stereoscopy,^{4–6} tomosynthesis,⁷ and 3D image reconstruction,⁸ which are expected to provide more diagnostic information about normal and abnormal tissue structure. It is

essential in the development of such systems to have a tool that can be used to test the visibility of breast structures and help select optimal views for 3D reconstruction, since the number of views is limited by the amount of radiation received.

Historically, mammography simulation started with the design of the first mathematical breast models for computing the dose received by a patient during an examination using Monte Carlo simulation of x-ray interactions.⁹ These simulations have used fairly crude models of breast anatomy, lacking internal structures. More recent analytical models of mammographic image acquisition have related the average values of the incident x-ray flux, linear attenuation coefficients of breast tissue, and the film density or pixel digital values in the obtained mammograms.¹⁰

There are two approaches to modeling the image content of mammograms. In a 2D approach, mammograms are modeled based upon the analysis of spatial correlation between image pixel values, using various random field methods.^{11–13} Such models can match some of the statistical properties of real mammograms, but they cannot reveal the relationship between the 3D structures of the breast, nor they can consistently produce images of the same breast with modified position or acquisition parameters.

In this paper we propose a second approach, whereby mammograms are modeled by projection of simulated 3D anatomic structures, based upon the size and the distribution of large and medium scale tissue regions found in the breast. It is our hypothesis that the distribution of the 2D structures seen in mammograms reflects the distribution of the 3D tis-

Mammography Simulation

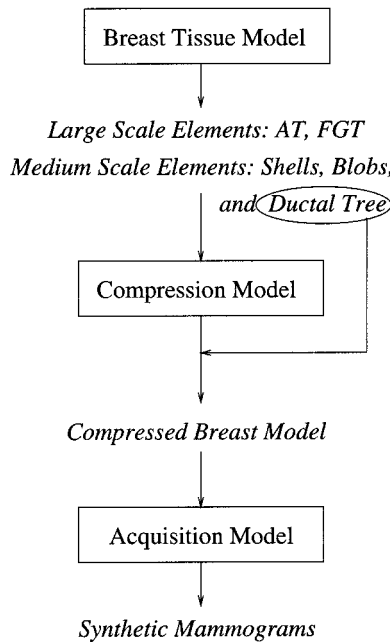


FIG. 1. Components of a system for mammography simulation. The flowchart shows the order (top-to-bottom) in which the model components are simulated.

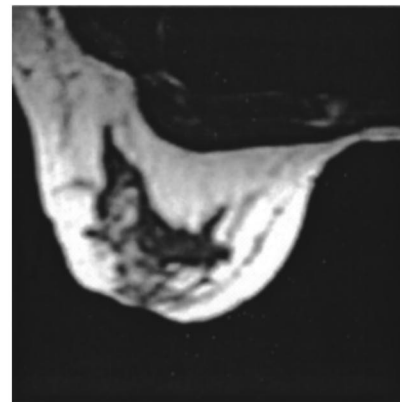
sue structures of the breast. Thus, the background texture in the synthetic mammograms so generated, should have similar properties to those found in clinical images.

Positioning and compression significantly affect the appearance of mammograms. Until recently^{14–16} there were no models of breast deformation, due to the complex anatomy of the different types of interwoven breast tissue, whose mechanical properties are difficult to analyze. We have approximated breast compression by separate deformations of tissue layers positioned normal to the compression plates.

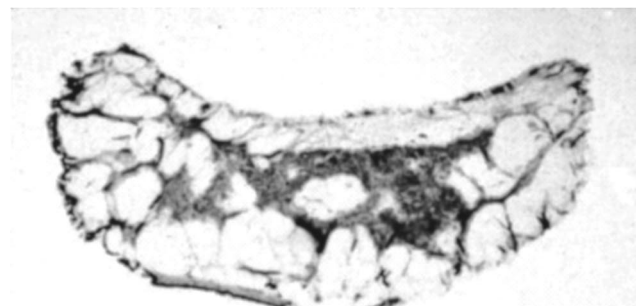
The objective of this work is to generate synthetic mammograms. A method for achieving this goal is described in Sec. II, while the results of the simulation are shown in Sec. III. An accompanying paper details an analysis of the quality of the model.¹⁷

II. MAMMOGRAPHY SIMULATION

The proposed mammography simulation consists of three major components: a 3D software breast phantom, a compression model, and an x-ray image acquisition model (see Fig. 1). The breast phantom is a software tissue model containing two ellipsoidal regions of large scale tissue elements: predominantly adipose tissue (AT) and predominantly fibroglandular tissue (FGT). The internal tissue structures of these regions, namely the adipose compartments and the breast ductal network, are approximated by realistically distributed medium scale phantom elements: shells, blobs, and the simulated ductal tree. The compression model is based upon tissue elasticity properties and a breast deformation model. Deformation is simulated separately for tissue slices (or layers)



(a)



(b)

FIG. 2. Anatomic structures of the breast included in the tissue model. (a) Large scale regions seen in MRI images as predominantly adipose tissue region, AT (bright), and predominantly fibroglandular region, FGT (dark surrounded by the AT). (b) Subgross (thick) histologic slice showing large scale regions: AT and FGT, and medium scale tissue structures: compartments surrounded by Cooper's ligaments in the AT and small adipose cavities and ducts within the FGT. (Subgross breast histology image provided courtesy of Dr. R. D. Cardiff.)

positioned normal to the compression plates. Each slice is approximated by a beam composed of two different tissues. Deformed slices are stacked to produce a model of the compressed breast. The mammogram acquisition model was adopted from the literature,¹⁰ assuming monoenergetic x rays and a parallel beam geometry without scatter. Presently, the synthetic mammograms are generated with a spatial resolution of $200 \mu\text{m}/\text{pixel}$ because the current model version does not include fine tissue details. This resolution is comparable to the resolution of digitized mammograms in the Mini MIAS database (obtained by averaging 4×4 pixels in the original MIAS database¹⁸).

A. Software breast phantom

1. Modeling large scale tissue regions

Figure 2 illustrates the types of anatomic structures of the breast which are included in the breast phantom. Figure 2(a) is an MRI breast section, showing the shape and position of

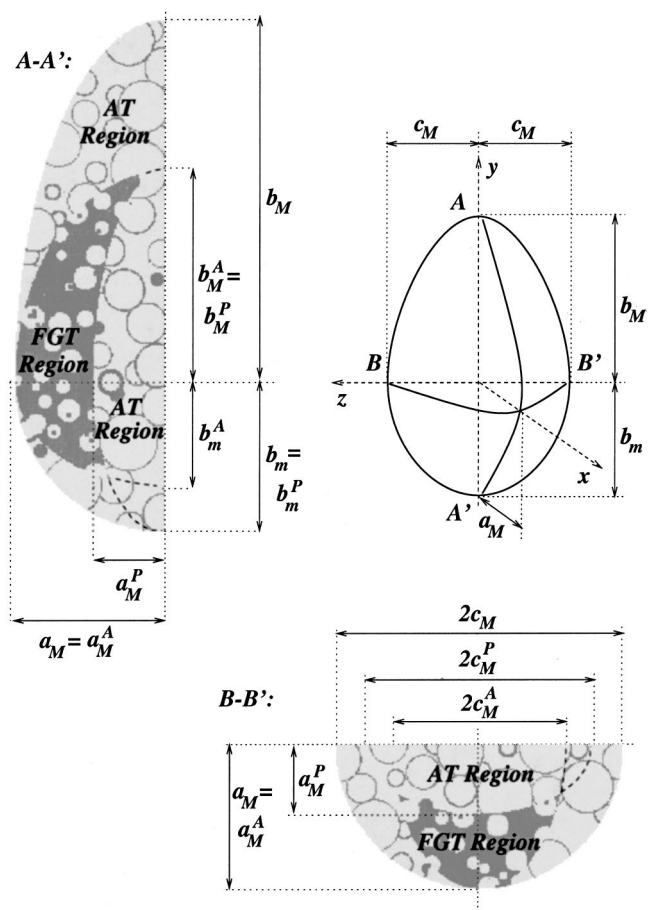


FIG. 3. Orthogonal sections of the uncompressed breast model. Parameters without subscripts correspond to the semi-axes of the ellipsoidal approximation of the breast outline; superscripts *A* and *P* correspond to the anterior and posterior border of the FGT model region, respectively.

the large scale tissue regions. The MRI shows the predominantly fibroglandular tissue, appearing as a dark region in the central part of the breast, and the predominantly adipose tissue, a brighter region surrounding the fibroglandular tissue. Internal structures of these tissue regions are less clearly visible, due to the relatively low MRI resolution of approximately 1 mm/pixel. Figure 2(b) shows a subgross histologic slice of the breast, obtained after mastectomy. The predominantly fibroglandular region in the slice is represented by a darker image region in the center, surrounded by brighter, predominantly adipose tissue. Adipose tissue is organized into round compartments, formed by fibrous Cooper's ligaments. The FGT region also contains adipose compartments, but they are smaller in size than the compartments in the AT region. Analysis of subgross histologic slices of the breast and the corresponding mammograms showed that projections of these compartments dominantly contribute to the formation of parenchymal patterns. Therefore, simulated adipose compartments were included as medium scale breast model elements.

2. Modeling adipose tissue compartments

The adipose compartments are approximated by thin shells in the AT region and small blobs in the FGT region.

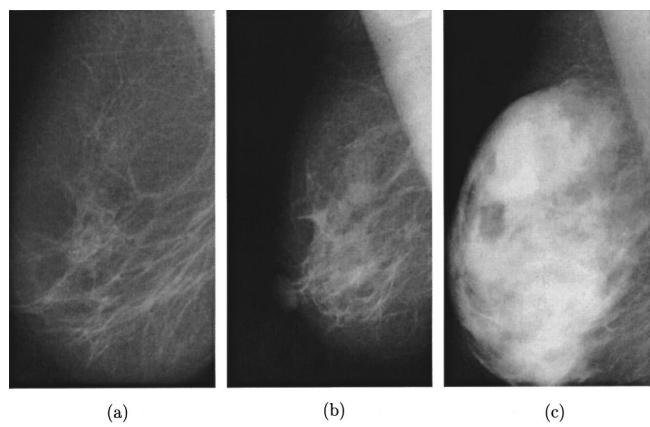


FIG. 4. Examples of different tissue distributions in real breasts, illustrated with clinical mammograms from the MIAS database. The amount of adipose tissue affects the size and visibility of compartments seen in the AT and FGT regions.

The interiors of the shells and blobs have the elastic and x-ray attenuation properties of adipose tissue. As a first approximation, the adipose compartments are represented by spheres. The size of the spheres can vary to allow for normal breast anatomic variations.

Figure 3 shows two orthogonal cross sections of a breast tissue phantom. Simulated regions of predominantly adipose and predominantly fibroglandular tissue are seen, together with the spherical approximation of adipose compartments in those regions. Note that the size of the simulated compartments in the AT and FGT regions differ. The size of the adipose compartments varies in different women, depending upon the amount of adipose tissue in the breast, as seen in

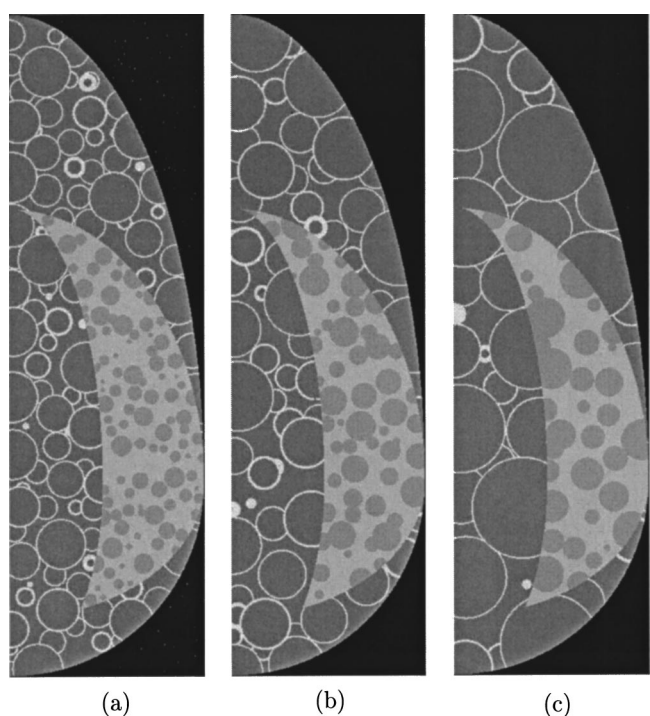


FIG. 5. Sections of breast models with different sized tissue elements labeled according to Table I as: (a) "Small," (b) "Medium," and (c) "Large."

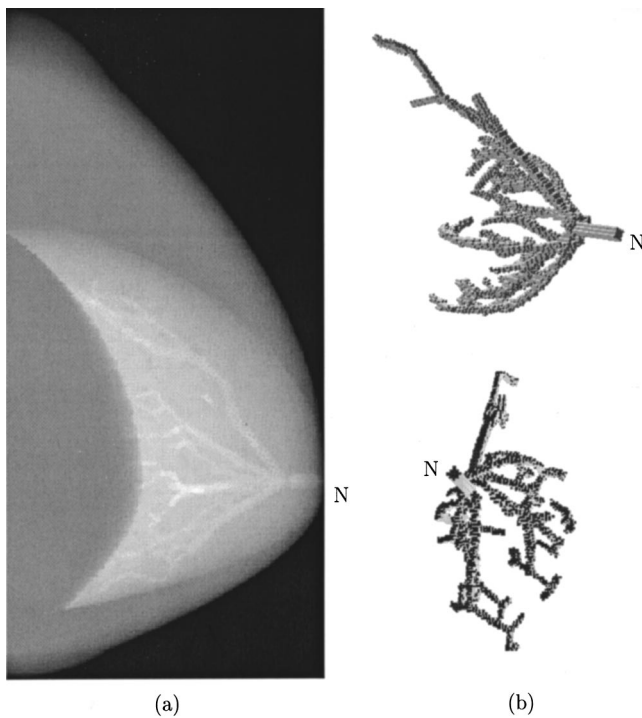


Fig. 6. Examples of computer generated ductal lobes. (a) A simulated mammogram with five duct lobes. For the purpose of this illustration, other medium scale image elements have been suppressed. (b) Two views of the same simulated ductal network, used to generate image in (a). (The letter "N" indicates position of the nipple.)

Fig. 4. Adipose compartments are more easily identified in a histologic slice than in a mammogram, since the latter image contains the superimposed projections of many tissue layers. Simulations of breasts with different sized adipose compartments are illustrated in Fig. 5. The procedure for generating simulated tissue compartments starts by filling the 3D breast phantom with compartments of the largest selected size until they start to intersect each other. The compartment size is then reduced and the procedure continued until the smallest selected size has been reached.

3. Modeling breast ductal network

To achieve a sufficiently realistic tissue phantom it is also necessary to model the breast ductal network. Ducts can be visualized by galactography, a clinical x-ray imaging procedure whereby the ducts are enhanced by injection of a contrast agent. The breast ductal system consists of about 15–20 ductal lobes, each corresponding to a major duct branching from the nipple into a network of smaller ducts. In galactograms, usually a single lobe is enhanced. Larger ducts are more visible than the smaller ones, since they attenuate more x rays.

The main focus of our model is on the pattern of duct branching. This pattern can be expressed by a ramification matrix, representing probabilities of branching at different levels of a tree structure.¹⁹ There are no previous reports in the literature on analyzing the breast ductal network by ramification matrices. The class of random binary trees was cho-

sen for modeling the ducts since it offers the least constrained branching pattern.¹⁹ The ductal model consists of 15 lobes and each lobe is simulated by a different random binary tree. Different trees are generated by using different random number generator seeds. A simulated ductal network is shown in Fig. 6. For clarity, only 5 out of 15 lobes are visible.

B. Mammographic compression model

The mammographic compression simulation is based upon a deformation model including realistic tissue elasticity properties. Elasticity parameters of the tissue found in the literature vary significantly.^{20–22} One of the reasons for these variations is that the experiments for determining the elastic properties have been performed using small samples taken from a particular tissue type (e.g., adipose, fibroglandular, or cancerous). However, the breast is comprised of a complicated admixture of different tissues which affect the elastic behavior of the whole organ.

The parameters most often used for description of elastic properties are the Young's linear elasticity modulus, E , and the Poisson's ratio, ν , defined by

$$E = \frac{\sigma}{\epsilon} = \frac{F/A}{\Delta l/l}, \quad \nu = \frac{\Delta w}{\Delta l}. \quad (1)$$

The Young's modulus relates the strain, ϵ , as a measure of deformation (i.e., the fractional change in length $\Delta l/l$) and the stress, σ (the force F applied to the surface area A of the deformed object). The Poisson ratio, ν , is equal to the ratio of transverse contraction, Δw , to the elongation, Δl , of a deformed bar. It is usually assumed that human tissue can be approximated as an incompressible material, whose volume does not change during deformation.²⁰ For incompressible materials $\nu \approx 0.5$.

The other elasticity moduli used to describe the behavior of material are the bulk modulus, K , and shear modulus, G , which can be expressed using the values of E and ν :

$$K = \frac{E}{3(1-2\nu)}, \quad G = \frac{E}{2(1+\nu)}. \quad (2)$$

There is a relationship between the bulk elasticity modulus, K , material density, ρ , and the speed of sound through the material, v , given by

$$v \approx \sqrt{K/\rho}. \quad (3)$$

In the compression model, the elasticity parameter values of adipose and fibroglandular tissues were computed using the values of ultrasound velocity through various tissues found in the literature.²³

The Mammography Quality Standards Act²⁴ regulates the minimum and maximum breast compression to be used in mammography. In general, the mammography technician will apply the maximum force tolerated by the patient to achieve optimum quality mammograms. Sullivan *et al.*²⁵ reported a statistical analysis of the compression force and compressed breast thickness, measured during 560 exams. Simulated force values were selected to address these considerations.

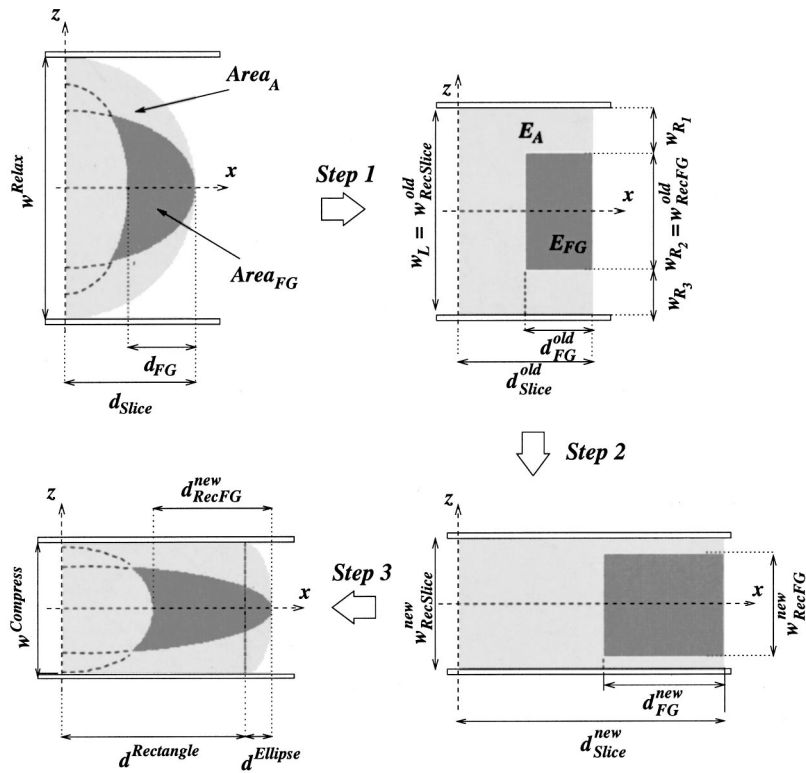


FIG. 7. Separate deformation of breast model slices. Illustrated are the steps of rectangular slice approximation, deformation of the approximated slice, and generation of the final shape of the deformed slice. These steps are followed by stacking all deformed slices together to generate the compressed breast shape (not shown).

There are very few published results about deformation of breast tissue structures during mammography. One reason is that it is hard to provide 3D visualization of such deformations. Clinically available 3D breast imaging techniques, ultrasound and MRI, have lower resolution and poorer quality than mammography. In addition, both methods use much less compression and are not applicable for analyzing tissue deformation during mammography. In our compression model, tissue deformation is estimated in two phases. First, the large scale model elements, the AT and FGT regions, are deformed to determine the shape of the compressed breast. Second, the medium scale model elements are deformed by transforming the shells and spheres into ellipsoids. After compression and x-ray image acquisition, the medium scale elements appear as elliptical structures in synthetic mammograms corresponding to the oval shaped lucencies seen in real mammograms.

The compression of large scale model elements is simulated in the form of separate deformations of the breast tissue slices, positioned normal to the compression plates. In this paper, the medio-lateral oblique (MLO) mammographic view is modeled since it provides visualization of more breast tissue than other views.²⁶ Moreover, in a number of countries, e.g., UK, the Netherlands, and Sweden, it is the only view obtained by breast screening.²⁷ Compression for other views, e.g., cranio-caudal (CC), can be simulated by a modification of the described model. In the case of MLO compression, tissue slices are positioned normal to the MLO view plane. In this case, a slice appears as a semiellipse, and the FGT portion of the slice appears as the intersection of two semiellipses, as shown in Fig. 3. Slice thickness corresponds to the model resolution specified at the beginning of the simulation.

Deformation of each slice is computed in three steps. First, a rectangular slice approximation is computed. Second, slice deformations are estimated using a composite beam model. Third, the compressed slice shape is computed from the deformed rectangular approximation. Compressed slices are stacked together to form the compressed breast model shape. A detailed description of the processing steps is given in the following.

1. Rectangular slice approximation

A slice of the breast model is replaced by its rectangular approximation. The whole slice region and its FGT portion are approximated by rectangles, satisfying the following constraints: (i) the area of the rectangular slice approximation, A_{Slice} , and area of the rectangular FGT approximation, A_{FG} , are the same as the corresponding areas in the original slice; (ii) the side of the rectangular slice approximation in the chest-nipple direction, d_{Slice} , and the side of the rectangular FGT approximation in the same direction, d_{FG} , are equal to the corresponding dimensions in the original slice; and (iii) the distance between the centers of gravity of the rectangular slice approximation and the rectangular FGT approximation is the same as the corresponding distance in the original slice. This constraint is not used for deformation of the slice through the nipple, because it may produce a rectangular approximation of the FGT region protruding outside of the slice. Instead, the FGT region is positioned so that it touches the nipple side of the rectangular approximation of the whole slice.

Using these constraints, the dimensions and relative positions of the rectangular slice and FGT approximation are

computed. An example of a slice through the nipple is illustrated in Fig. 7.

2. Slice deformation via a composite beam model

The approximating rectangles preserve the elastic properties of the corresponding slice regions. The elastic properties of the AT and FGT regions are modeled by linear Young's moduli, E_A and E_{FG} , respectively. This rectangular slice approximation can be treated as a composite 2D elastic beam, positioned between two bars corresponding to slices through the compression plates. Deformation is estimated by applying a force to the compression plates which in turn deforms the composite beam. It is assumed that (i) the slice thickness is much smaller than the sides of the approximating rectangles and (ii) during the compression, the slice stays in the same plane as before compression. The latter assumption is based on the fact that in reality slices of tissue are not compressed independently; the neighboring tissue (above or below) partially confine the slice to a plane. Slices in the planes above or below the nipple level do not have initial contact with the compression plates. It is assumed that all slices deform with the same strain value which is equal to the strain of the slice in the nipple level:

$$\epsilon_{Slice} = \epsilon_{Nipple}^{Nipple} = \frac{\Delta w_{RecSlice}}{w_{RecSlice}} = 1 - \frac{w_{RecSlice}^{new}}{w_{RecSlice}^{old}} = 1 - \frac{w^{Compress}}{w^{Relax}}, \quad (4)$$

where ϵ_{Slice} and $\epsilon_{Nipple}^{Nipple}$ represent strain for any slice and strain for the slice in the nipple level, respectively; $w_{RecSlice}^{old}$ and $w_{RecSlice}^{new}$ represent size of the rectangular approximation normal to the compression plates, before and after compression, respectively; w^{Relax} and $w^{Compress}$ represent breast thickness before and after compression, respectively. The intensity of the compression force is included indirectly, by specifying the thickness of the compressed breast. Since a linear model of tissue elasticity is used, only the ratio of Young's moduli for the AT and FGT region is needed to estimate slice deformation.

The stress in the rectangular FGT region, σ_{R_2} , is the same as the stresses σ_{R_1} and σ_{R_3} in the parts of the rectangular AT region with thickness w_{R_1} and w_{R_3} ,

$$\sigma_{R_1} = \sigma_{R_2} = \sigma_{R_3}. \quad (5)$$

Replacing σ_i by $E_i\epsilon_i$, from Eq. (1), the strain in the rectangular FGT approximation is calculated as:

$$\epsilon_{R_2} = \frac{E_A}{E_{FG}} \epsilon_{R_1}. \quad (6)$$

The ratio E_A/E_{FG} is computed based upon the relationship between the bulk elastic moduli, tissue density, and velocity of sound propagation through the tissue. Measured values of the velocity of sound in samples of adipose and fibroglandular tissue are $v_A = 1470$ m/s and $v_{FG} = 1545$ m/s, respectively.²³ Densities of the adipose and fibroglandular tissue are $\rho_A = 930$ kg/m³ and $\rho_{FG} = 1040$ kg/m³, respectively.²⁸ Using Eq. (3), gives

$$\frac{E_A}{E_{FG}} \approx \frac{K_A}{K_{FG}} \approx \frac{\rho_A v_A^2}{\rho_{FG} v_{FG}^2} = 0.81. \quad (7)$$

Finally, there is a relationship between the strains in different parts of the rectangular slice approximation, since:

$$\Delta w_L = \Delta w_{R_1} + \Delta w_{R_2} + \Delta w_{R_3}, \quad (8)$$

which after dividing by w_L and using the fact that $\epsilon_{R_1} = \epsilon_{R_3}$ due to symmetry, yields

$$\epsilon_L = \epsilon_{R_1} \frac{w_{R_1} + w_{R_3}}{w_L} + \epsilon_{R_2} \frac{w_{R_2}}{w_L}. \quad (9)$$

Equations (4), (6), and (9) yield dimensions of the rectangular slice and FGT region normal to the compression plates after the compression, $w_{RecSlice}^{new}$ and w_{RecFG}^{new} , respectively:

$$w_{RecSlice}^{new} = w_L(1 - \epsilon_L), \quad w_{RecFG}^{new} = w_{R_2}(1 - \epsilon_{R_2}). \quad (10)$$

Assuming that the areas of the rectangular slice and FGT region, A_{Slice} and A_{FG} , stay the same before and after compression, we can compute the dimension of the rectangular slice and FGT approximation in the chest-nipple direction after compression, $d_{RecSlice}^{new}$ and d_{RecFG}^{new} , respectively:

$$d_{RecSlice}^{new} = \frac{A_{Slice}}{w_{RecSlice}^{new}}, \quad d_{RecFG}^{new} = \frac{A_{FG}}{w_{RecFG}^{new}}. \quad (11)$$

3. Compressed slice from the deformed rectangular approximation

The final step of the slice deformation modeling is the computation of the compressed breast slice from its deformed rectangular approximation. The compressed breast does not have an ellipsoidal but rather a flattened shape.^{26,29} The thickness of the compressed breast is constant and equal to the distance between the compression plates, $w^{Compress}$, everywhere except in a narrow region close to the front edge of the breast. Analysis of that region on a mammogram was used to estimate the breast thickness directly from mammograms.³⁰ To achieve a realistic shape of the compressed breast slice, a correction was applied to the model.³¹ This correction assumes that the deformed breast slice consists of a rectangle positioned at the chest wall side, and a semiellipse attached to the rectangle, extending forward to the nipple (see Fig. 7).

Parameters of the deformed rectangle and semiellipse are computed satisfying the following constraints: (i) the sum of the rectangular area, $A^{Rectangle}$, and the semielliptical area, $A^{Ellipse}$, is equal to the area of the whole uncompressed slice, A_{Slice} ; (ii) one side of the rectangle and one axis of the semiellipse are equal to the distance between the compression plates for the compressed breast, $w^{Compress}$; and (iii) the slice region where the thickness is less than $w^{Compress}$ contains 10% of the whole mammogram breast area.³⁰ The described correction for flattening the compressed breast is

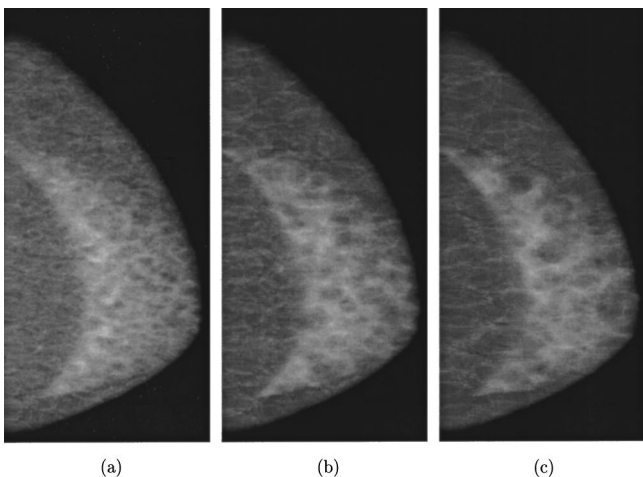


FIG. 8. Examples of synthetic images with different sizes of tissue model elements (i.e., simulated compartments in the AT and FGT), which are used for comparison with clinical mammograms. The images are labeled according to Table I as: (a) “Small,” (b) “Medium,” and (c) “Large.”

only used to determine the border of the whole compressed slice. Deformation of the FGT region is still computed using the 2D composite beam approximation.

Separate processing of individual model slices is followed by stacking the deformed slices together to get the 3D compressed breast model. Slices whose relaxed (noncompressed) thickness is less than the compressed breast thickness are not processed at all; they are assumed to preserve their relaxed shape. The compressed breast thickness was used instead of the compression force to compute the deformation of the breast model slices. The compression force can be calculated from the difference of the relaxed and compressed breast thickness and tissue elastic moduli using Hooke’s law. When computing the force, the values for both the elastic moduli of the adipose and fibroglandular tissue are needed.

C. X-ray mammogram acquisition model

The x-ray image acquisition model consists of an x-ray propagation model, which includes attenuation by the breast tissue and conversion of the x-ray energy into film density, and a model of mammographic film digitization. In the case of digital mammography, the film and digitization models should be replaced by a model of a solid-state x-ray detector array. The model is adopted from the literature,¹⁰ and for simplicity assumes a monoenergetic x-ray spectrum and a parallel beam geometry, without scatter.

The mammogram acquisition model relates the spatial distribution of the x-ray energy imparted to the intensifying screen, E_I , to the mammogram digital values (after digitization), DV, and the linear x-ray attenuation coefficient of tissue, μ_t :

$$E_I(x,y) = \eta \phi E C \exp \left\{ - \int_{z=0}^{z=w^{\text{Compress}}} \mu_t(x,y,z) dz \right\}, \quad (12)$$

$$DV(x,y) = a - b \gamma \log_{10}\{\beta E_I(x,y)\}, \quad (13)$$

TABLE I. Radii of simulated adipose compartments in the AT and FGT, used to generate the synthetic mammograms.

Structure radii	Model regions	
	AT (mm)	FGT (mm)
Small	2.7–6.7	1.3–2.7
Medium	4–10	2–4
Large	5.3–13.3	2.7–5.3

where η represents the quantum efficiency of the screen, ϕ is the fluence at the entrance to the breast, E the x-ray photon energy, C is the attenuation factor due to the compression paddle and grid, w^{Compress} is the compressed breast thickness, a and b are digitization coefficients, and γ and β are the film gamma and the speed coefficient, respectively. It is assumed that the digitization output is proportional to optical density, thus Eqs. (12) and (13) can be simplified so that DV is linearly proportional to the ray sum. The linear x-ray attenuation coefficients of the AT and FGT tissue, taken from the literature,³² are $\mu_{\text{AT}}=0.456 \text{ cm}^{-1}$ and $\mu_{\text{FG}}=0.802 \text{ cm}^{-1}$, at 20 keV. Further details of the acquisition model are given in the literature.³³

III. SIMULATION RESULTS AND DISCUSSION

Figure 8 shows three synthetic mammograms generated by our simulation. These three images differ in the size of the simulated medium scale tissue structures. The ranges of adipose compartments radii simulated in the mammograms (shown in Fig. 8) are given in Table I.

It can be noted that the proportions of the breast model, i.e., vertical to horizontal dimension ratio after compression, agree with the “standard breast” from Novak,²⁹ defined by averaging dimensions of 27 compressed breasts. Dimensions of the breast model are smaller than the “standard breast” by approximately 15%.

The synthetic mammograms were printed on film (AGFA LR5200, AGFA-Gevaert, Belgium) lifesize, and were shown to radiologists in the Breast Imaging Center of Thomas Jefferson University. Qualitatively, subregions of synthetic and clinical images were reported to have similar appearance when viewed at a distance of 1–2 m. When examined closely, it was observed that the synthetic images lack blood vessels and other organized fine tissue structures. In addition, the borders between the AT and FGT regions in the synthetic mammograms appeared as a clear, geometrically regular separation degrading the subjective perception of reality. For the latter reason, the model was modified by addition of small random variations to the position of the borders between the compressed AT and FGT phantom regions. This correction is included in Fig. 8.

As stated in Sec. I, the model for producing the synthetic mammograms was based upon the hypotheses that the size and the distribution of simulated 3D tissue elements are similar to those found in the real breasts, and that the 3D tissue distribution is reflected in the distribution of 2D mammographic structures. In order to evaluate the synthetic images,

we performed statistical comparisons of several texture descriptors computed in synthetic and clinical mammograms, including: average size of image objects, texture energy, and fractal dimension. These descriptors have been previously used in the literature for the analysis of parenchymal patterns in mammograms.^{34–36} The image objects' size, analyzed using mathematical morphology, can be related to the size of the simulated 3D tissue structures. Texture energy and fractal dimension are sensitive to small scale changes in image intensities, corresponding to fine tissue detail. Details about the texture analysis of synthetic and clinical mammograms are given in the accompanying paper.¹⁷ Quantitatively, the synthetic mammograms have a similar distribution of values averaged over a large number of clinical mammograms. The best matching was observed for the synthetic images generated using the simulated adipose compartments with radii of 4–13.3 mm in the AT regions, and radii of 2.7–5.33 mm and 1.3–2.7 mm in the retroareolar and dense FGT regions, respectively.¹⁷ It is expected that the introduction of detailed tissue structures in the breast model will enhance the local variations of synthetic mammograms and the variations in feature distribution needed to better match real images. In addition, the simulated ducts and the compression model were separately evaluated and compared with clinically acquired data.^{33,37}

IV. CONCLUSIONS

A method is described for generating synthetic mammograms using simulations of breast tissue and the mammographic imaging process. A software breast phantom was developed, which contains realistic large and medium scale tissue structures, derived from an understanding of the macroscopic anatomic tissue organization. Parameters controlling the size and placement of the tissue simulating structures provide flexibility to generate a large database of synthetic images with different characteristics. Mammographic imaging is simulated using a compression model and a model of the x-ray image acquisition. The compression model estimates breast deformation using tissue elasticity parameters found in the literature and realistic values of compression force. The synthetic mammograms were generated by a mammogram acquisition model using a monoenergetic parallel beam approximation, applied to the synthetically compressed breast phantom.

The proposed simulation can be used in analysis of breast positioning, compression, and image acquisition parameters. The software breast phantom can be used as a test object for optimizing mammographic systems or testing novel systems for 3D reconstruction of breast images. The simulation can be used for analyzing the correlation between the 3D breast composition and 2D mammogram characteristics, e.g., the parenchymal patterns, which can be used for estimation of the cancer risk.³⁸ Computer algorithms for characterization of normal breast tissue could be tested on large databases of normal images with random variations of tissue structures, generated by the model. Synthetic mammograms with simulated abnormalities or abnormalities extracted from clinical

mammograms could be used for testing algorithms for cancer detection.

ACKNOWLEDGMENTS

This work was supported in part by NSF Grant No. IRI-9504363 and by US Army Breast Cancer Research Program Grant Nos. DAMD 17-96-1-6128 and DAMD 17-98-1-8169. The authors would like to thank Dr. Robert D. Cardiff, University of California, Davis, for providing the images of breast subgross histology specimens.

^{a)}Author to whom all correspondence should be addressed; electronic mail: Andrew.Maidment@mail.tju.edu

¹J. P. Rolland and H. H. Barrett, "Effect of random background inhomogeneity on observer detection performance," *J. Opt. Soc. Am. A* **9**, 649–658 (1992).

²F. O. Bochud, J.-F. Valley, F. R. Verdun, C. Hessler, and P. Schnyder, "Estimation of the noisy component of anatomical background," *Med. Phys.* **26**, 1365–1370 (1999).

³A. E. Burgess, F. L. Jacobson, and P. F. Judy, "Human observer detection experiments with mammograms and power-law noise," *Med. Phys.* **28**, 419–437 (2001).

⁴J. Hsu, D. M. Chelberg, C. F. Babbs, Z. Pizlo, and E. Delp, "Preclinical ROC studies of digital stereomammography," *IEEE Trans. Med. Imaging* **14**, 318–327 (1995).

⁵M. M. Goodlett, H.-P. Chan, and L. Hadjiiski, "Stereomammography: Evaluation of depth perception using a virtual 3D cursor," *Med. Phys.* **27**, 1305–1310 (2000).

⁶P. R. Bakic, M. Albert, and A. D. A. Maidment, "Dose requirements in stereoradiography," in *Physics of Medical Imaging*, edited by L. E. Antonuk and M. J. Yaffe [Proc. SPIE **4682**, 126–137 (2002)].

⁷L. T. Niklason *et al.*, "Digital tomosynthesis in breast imaging," *Radiology* **205**, 399–406 (1997).

⁸A. D. A. Maidment, M. Albert, and E. F. Conant, "Three-dimensional imaging of breast classifications," in *Exploiting New Image Sources and Sensors*, edited by J. M. Selander [Proc. SPIE **3240**, 200–208 (1997)].

⁹K. Doi and H.-P. Chan, "Evaluation of absorbed dose in mammography," *Radiology* **135**, 199–208 (1980).

¹⁰R. P. Highnam, J. M. Brady, and B. J. Sheppstone, "Computing the scatter component of mammographic images," *IEEE Trans. Med. Imaging* **13**, 301–313 (1994).

¹¹F. O. Bochud, C. K. Abbey, and M. P. Eckstein, "Statistical texture synthesis of mammographic images with clustered lumpy backgrounds," *Opt. Express* **4**, 33–43 (1999).

¹²H. D. Li, M. Kallergi, L. P. Clarke, V. K. Jain, and R. A. Clark, "Markov random field for tumor detection in digital mammography," *IEEE Trans. Med. Imaging* **14**, 565–576 (1995).

¹³J. J. Heine, S. R. Deans, R. P. Velthuizen, and L. P. Clarke, "On the statistical nature of mammograms," *Med. Phys.* **26**, 2254–2265 (1999).

¹⁴P. Bakic, D. Brzakovic, and Z. Zhu, "Anatomic segmentation of mammograms via breast model," in *Digital Mammography Nijmegen, 1998*, Proceedings of the Fourth International Workshop on Digital Mammography, Nijmegen, The Netherlands, June 1998, edited by N. Karssemeijer, M. Thijssen, J. Hendriks, and L. van Erning (Kluwer Academic, Dordrecht, 1998), pp. 291–294.

¹⁵Y. Kita, R. Highnam, and M. Brady, "Correspondence between different view breast x-rays using a simulation of breast deformation," Proceedings of the IEEE Computer Vision and Pattern Recognition Conference, Santa Barbara, CA, June 1998, pp. 700–707.

¹⁶A. Samani, J. Bishop, E. Ramsey, and D. B. Plewes, "A 3-D contact problem finite element model for breast shape deformation derived from MRI data," Proceedings of the 23rd Annual Meeting of the American Society of Biomechanics, Pittsburgh, October 1999.

¹⁷P. R. Bakic, M. Albert, D. Brzakovic, and A. D. A. Maidment, "Mammogram synthesis using 3D simulation. II. Evaluation of synthetic mammogram texture," *Med. Phys.* **29**, 2140–2151 (2002).

¹⁸J. Suckling *et al.*, "The Mammographic Image Analysis Society Digital Mammogram Database," in *Digital Mammography*, Proceedings of the Second International Workshop on Digital Mammography, York,

- England, 10–12 July 1994, edited by A. G. Gale, S. M. Astley, D. R. Dance, and A. Y. Cairns (Elsevier Science, Amsterdam, 1994), p. 375–378 (<http://www.wiau.man.ac.uk/services/MIAS/MIASmini.html>)
- ¹⁹X. G. Viennot, G. Eyrrolles, N. Janey, and D. Arques, “Combinatorial analysis of ramified patterns and computer imagery of trees,” *Comput. Graph.* **23**, 31–40 (1989).
- ²⁰A. P. Sarvazyan, A. R. Skorovoda, S. Y. Emelianov, J. B. Fowlkes, J. G. Pipe, R. S. Adler, R. B. Buxton, and P. L. Carson, “Biophysical bases of elasticity imaging,” in *Acoustic Imaging*, edited by J. P. Jones (Plenum, New York, 1995), pp. 223–240.
- ²¹F. S. Azar, D. Metaxas, and M. D. Schnall, “A finite model of the breast for predicting mechanical deformations during interventional procedures,” *Proceedings of the International Symposium on Magnetic Resonance in Medicine*, Philadelphia, PA, May 1999.
- ²²A. Samani, J. Bishop, E. Ramsey, and D. B. Plewes, “Breast tissue deformation finite element modeling for MRI/x-ray mammography data fusion,” in *Digital Mammography, IWDM 2000, Toronto, Canada*, Proceedings of the Fifth International Workshop on Digital Mammography, edited by M. J. Yaffe (Medical Physics Publishing, Madison, WI, 2001), pp. 763–769.
- ²³G. Kossoff, E. K. Fry, and J. Jellins, “Average velocity of ultrasound in the human female breast,” *J. Acoust. Soc. Am.* **53**, 1730–1736 (1973).
- ²⁴ACR Committee on Quality Assurance in Mammography, *Mammography Quality Control Manual* (American College of Radiology, Reston, VA, 1999).
- ²⁵D. C. Sullivan, C. A. Beam, S. M. Goodman, and D. L. Watt, “Measurement of force applied during mammography,” *Radiology* **181**, 355–357 (1991).
- ²⁶G. W. Eklund and G. Cardenosa, “The art of mammographic positioning,” *Radiol. Clin. North Am.* **30**, 21–53 (1992).
- ²⁷B. Lundgren and S. Jakobsson, “Single view mammography,” *Cancer* **38**, 1124–1129 (1976).
- ²⁸G. R. Hammerstein *et al.*, “Absorbed radiation dose in mammography,” *Radiology* **130**, 485–491 (1979).
- ²⁹R. Novak, “Transformation of the female breast during compression at mammography with special reference to the importance for localization of a lesion,” *Acta Radiol., Suppl.* **371**, 7–46 (1988).
- ³⁰R. Highnam, M. Brady, and B. Sheppstone, “Estimating compressed breast thickness,” in *Digital Mammography Nijmegen, 1998*, Proceedings of the Fourth International Workshop on Digital Mammography, Nijmegen, The Netherlands, June 1998, edited by N. Karssemeijer, M. Thijssen, J. Hendriks, and L. van Erning (Kluwer Academic, Dordrecht, 1998), pp. 275–278.
- ³¹P. Bakic and D. Brzakovic, “Simulation of digital mammogram acquisition,” in *Physics of Medical Imaging*, edited by J. M. Boone and J. T. Dobbins III [Proc. SPIE **3659**, 866–877 (1999)].
- ³²P. C. Johns and M. Yaffe, “X-ray characterization of normal and neoplastic breast tissue,” *Phys. Med. Biol.* **32**, 675–695 (1987).
- ³³P. R. Bakic, “Breast tissue description and modeling in mammography,” Ph.D. dissertation, Lehigh University, Bethlehem, PA, 2000.
- ³⁴S. Behrens and J. Dengler, “Analyzing the structure of medical images with morphological size distributions,” *Proceedings of the Tenth International Conference on Pattern Recognition*, Atlantic City, NJ, June 1990, pp. 886–890.
- ³⁵P. I. Miller and S. M. Astley, “Classification of breast tissue by texture analysis,” *Image Vis. Comput.* **10**, 277–282 (1992).
- ³⁶C. B. Caldwell, S. J. Stapleton, D. W. Holdsworth, R. A. Jong, W. J. Weiser, G. Cooke, and M. J. Yaffe, “Characterization of mammographic parenchymal pattern by fractal dimension,” *Phys. Med. Biol.* **35**, 235–247 (1990).
- ³⁷P. R. Bakic, M. Albert, and A. D. A. Maidment, “Evaluation of breast ductal networks using ramification matrices,” in *IWDM 2002*, Proceedings of the Sixth International Workshop on Digital Mammography, Bremen, Germany, June 2002.
- ³⁸J. W. Byng, M. J. Yaffe, R. A. Jong, R. S. Shumak, G. A. Lockwood, D. L. Trichler, and N. F. Boyd, “Analysis of mammographic density and breast cancer risk from digitized mammograms,” *Radiographics* **18**, 1587–1598 (1998).